RESEARCH

Photocatalytic, Antibacterial, Cytotoxic and Bioimaging Applications of Fluorescent CdS Nanoparticles Prepared in DNA Biotemplate

V. N. Reena[1,2] · G. S. Bhagyasree[1,2] · T. Shilpa[3] · R. Aswati Nair[3] · H. Misha[4,5] · B. Nithyaja[1,2]

Abstract

Synthesizing nanoparticles in biotemplates has been cited as one of the most promising way to obtain monodispersed inorganic nanoparticles. In this method, uniform voids in porous materials serve as hosts to confine the synthesized nanoparticles. DNA template can be described as a *smart glue* for assembling nanoscale building blocks. Here we investigate the photocatalytic, antibacterial, cytotoxic, and bioimaging applications of DNA capped CdS. XRD, SEM, TEM, UV–visible absorption, and photoluminescence spectra were used to study structural, morphological, and optical properties of CdS nanoparticles. Prepared CdS nanoparticles exhibit visible fluorescence. The photocatalytic activity of CdS towards Rhodamine 6G and Methylene blue are 64% and 91% respectively. A disc-diffusion method is used to demonstrate antibacterial screening. It was shown that CdS nanoparticles inhibit Gram-positive bacteria and Gram-negative bacteria effectively. DNA capped CdS shows higher activity than uncapped CdS nanoparticles. MTT cell viability assays were carried out in HeLa cells to investigate the cytotoxicity for 24 h. At a concentration 2.5 µg/ml, it shows 84% cell viability and 43% viability at 12.5 µg/ml. The calculated LC_{50} value is equal to 8 µg/ml. These DNA capped CdS nanoparticles were taken for an in-vitro experiment with HeLa cells to exhibit the possibility of bioimaging applications. The present study suggests that the synthesized CdS nanoparticles could be a potential photocatalyst, antibacterial agent, and biocompatible nanoparticle for bioimaging applications.

Keywords Biotemplate · DNA · Nanoparticles · Photocatalysis · Photoluminescence · Bioimaging

Introduction

DNA, the bio-organic polymer, is an important biotemplate for synthesizing inorganic nanomaterials due to its well-defined sequence of DNA bases and super helix structures. Experiments on the preparation of nanomaterials found that DNA could act as *smart glue* for gathering nanoparticles [1–5]. The development of functionalized nanomaterials using proteins, peptides, and nucleic acids is the current advance in biotechnology. Many metal nanoparticles and semiconductor nanoparticles were effectively prepared using DNA biotemplate. Metal nanoparticles of gold, silver, nickel, palladium, copper, and platinum, and semiconductor nanoparticles of cerium oxide, CdS, were synthesized using a DNA template [1–4, 6–8].Phosphate groups are arranged regularly in the two backbones of DNA double helices, creating a negative charge on the chain. Highly charged double helical chain exhibits local stiffness in a range of about 50 nm but long-range flexibility in the water. Therefore, DNA is an ideal template for fabricating highly organized nanostructures with cationic binding agents such as metal ions, cationic surfactants, and polycationic agents.

CdS nanoparticles are II-VI group semiconductor materials having direct bandgap energy of 2.42 eV in the visible region at room temperature. Usually, CdS nanocrystals possess three types of crystal structures: cubic zinc blende, hexagonal wurtzite, and rock salt phase [9]. Several synthesis methods have been experimented with to control the size and growth of CdS nanoparticles. Sonochemical,

✉ V. N. Reena
rinanarayan@gmail.com

1 Photonic Materials Research Laboratory, Department of Physics, Government College Madappally, Vadakara, Kozhikode 673102, Kerala, India

2 University of Calicut, Malappuram 673635, Kerala, India

3 Department of Biochemistry and Molecular Biology, Central University of Kerala, Kasaragod 671316, Kerala, India

4 Department of Physics, Baselius College, Kottayam 686001, India

5 Mahatma Gandhi University, Kottayam 686560, India

microwave-solvothermal, and surfactant–ligand co-assisting solvothermal methods are some. For the preparation of nanoparticles, sonochemical (ultrasonic irradiation) is a simple and efficient method. During ultrasonic cavitation, many microbubbles form, grow and collapse within a few microseconds. By applying ultrasonic cavitation, a rigorous environment can be created by heating and cooling processes exceeding 109 K/s, in accordance with sonochemical theory calculations. Ultrasound breaks down nanoparticle aggregates by utilizing multiple effects [10].

Dye-containing wastewater demands highly effective treatment due to its acute toxicity. Several dyes are potentially canned annually from textile, ink, paper, pharmaceutical, cosmetic, and other industries [11–15]. Based on reduced time and energy efficiency procedures, photocatalysis was a good alternative to other methods [13, 14]. Recent research has ascertained that CdS NPs are good alternatives to photocatalysts [16–18].

The fluorescent behaviour of CdS nanoparticles has been taken advantage of in biomedical applications, and they have more advantages over conventional organic dyes, especially in bioimaging applications. CdS is a promising candidate for in-vivo and in-vitro imaging of normal and cancerous cells [19–21]. Incorporating nanoparticles into biological systems necessitates biocompatibility. To achieve biocompatibility, nanoparticles must be capped with natural or organic structures. Since DNA is a biological molecule, it may reduce the toxicity of CdS. Therefore, they may possess potential applications in bioimaging and associated applications.

In 2005, Kulkarni et al. reported a DNA-capped CdS nanoparticle in which they studied the interaction of Histone protein with CdS nanoparticles and investigated the photoluminescence variations [22]. In the wok by Ma et al., CdS nanocrystals with monomeric and oligomeric nucleic acid ligands are synthesized, and their properties are monitored as a function of the length and sequence of the passivating ligand. Monomeric nucleic acid such as ATP, GTP, CTP, or UTP and oligomeric nucleic acid of 18-mer DNA were used as ligands to synthesize CdS nanocrystals. Here in this work, we used double stranded DNA obtained from herring sperm. The helical structure of double stranded DNA possesses a wide major groove and a narrow minor groove. This makes small molecules to intercalate into the spaces between the stacked bases, or bind in the grooves between the two backbones. Both interaction patterns are highly selective toward the structure of the small molecules [23]. Yao et al. in 2008, CdS nanoparticles on DNA templates were synthesized by heating the DNA networks with Cd^{2+} in Thiourea [24]. In 2012, Nithyaja et al. followed the same procedure to synthesize CdS nanoparticles and studied the bandgap tunability, photoluminescence, and excitation wavelength dependency on fluorescence emission. They heat the salt solution along

with DNA up to 70 °C. Since heating causes denaturation of DNA, the capping action may not be 100% effective [25]. Previously we have reported the synthesis of DNA-capped CdS and investigated its effect on photoluminescence of Rhodamine 6G doped sol–gel derived glasses. We executed a co-precipitation method with ultrasonic irradiation using Cd^{2+} solution and Na_2S [26]. The capping agents are crucial in synthesizing highly mono-dispersed CdS nanoparticles by growth restriction methods. Several biocompatible capping agents are exploited to achieve growth restriction in preparation for CdS nanoparticles [25, 27–33]. Their chemical and physical properties strongly depend on size [34–36]. Their excellent properties have been exploited in applications like light-emitting diodes, lasers, sensors, solar cells, photocatalysis, photocells, display devices, invertors, waveguides, and bioimaging [37–42]. Although there are a few works on DNA-capped CdS nanoparticles, their biological and photocatalytic applications still need to be reported. Given the excellent properties of DNA-capped CdS nanoparticles, we explored their photocatalytic and biological applications. Therefore, we present in this paper the photocatalytic, antibacterial, cytotoxic, and bioimaging applications of CdS nanoparticles prepared in a DNA template.

Experimental

All chemicals cadmium nitrate (98%), sodium sulfide (99%), double-stranded DNA sodium salt derived from herring sperm, Rhodamine 6G dye (99%), Methylene blue ($\geq$ 95%) dye were obtained from Sigma Aldrich.

Synthesis of D-CdS Nanoparticles

A co-precipitation method is implemented to synthesize CdS nanoparticles. 50 mM Cadmium nitrate hexahydrate $(Cd(NO_3)2.6H_2O)$ was dissolved in 0.5 wt% DNA aqueous solution. While stirring continuously, 50 mM Sodium sulfide solution was added to this solution. After 30 min, a yellow-colored precipitate was obtained, indicating the formation of CdS nanoparticles. The precipitate was filtered, thoroughly washed with de-ionized water, and dried at 45 °C for further investigation [26].

The possible capping mechanism of the double stranded DNA is explained as follows: Sulfide ions in sodium sulfide will bind to Cd^{2+} ions bound on the phosphate groups of DNA, and the CdS nucleus is formed in the DNA network. DNA prevents the agglomeration and aggregation of CdS nanoparticles. As CdS nanoparticles form at room temperature, DNA retains its double-stranded structure, acting as a strong capping agent.

Measurements and Characterization of D-CdS

A Shimadzu UV-1800 UV–Vis Spectrophotometer, Japan, was used to obtain UV–Visible absorption spectra. Horiba Fluorolog 3 Fluorescence Spectrometer, Japan, was used to obtain fluorescence spectra. Powder XRD patterns of the samples were recorded at room temperature by Rigaku Ultima IV, Japan, X-ray diffractometer utilizing CuKα radiation ($\lambda = 1.54182$ Å) operating at 35 kV and 25 mA. A Floid Evos imaging system from Thermo Fisher Scientific, Nepal, was employed to record the cellular imaging of the sample at 20X magnification.

Photocatalytic Activity

The photodegradation of organic dye solutions by D-CdS was studied. We chose two organic dyes; Rhodamine 6G and Methylene blue. In this procedure, 10 mg of D-CdS is added to 100 ml of 10^{-5} M aqueous dye solutions and stirred under a dark environment for 30 min in an ultrasonicator, which ensure the adsorption–desorption equilibrium among the nanoparticles. UV light of wavelength 254 nm irradiation with continuous stirring was applied to the reaction mixture. The photocatalytic activity using UV irradiation and visible/solar light was done and compared the results. It was seen that the photocatalytic activity was lesser in the samples under solar irradiation than in the samples under UV irradiation. In a study [43], it was shown that the rate of degradation of pollutants was faster using UV than solar light. It is shown that shorter wavelengths have a greater chance of trapping electron–hole pairs than long wavelengths of visible light. Furthermore, only 5% of the solar spectrum contains UV light, limiting the potential for very good results.

The degradation of the dye solutions was monitored at regular intervals (0, 25, 50, 75, 100, and 120 min) using a UV–Vis spectrophotometer. The procedure is repeated without D-CdS to investigate the photocatalytic efficiency of D-CdS. The formula can find the percentage of photodegradation [44],

$$\% \ of degradation = \frac{A_0 - A_T}{A_0} \times 100$$

where A_0 is the initial absorbance of dye and A_T is the absorbance of the dye after irradiation in a particular time interval.

Antibacterial Activity

The antibacterials present in the samples can diffuse into the medium and interact in a plate freshly seeded with the test organisms. The resulting inhibition zones will be uniformly circular as there will be a confluent lawn of growth. Three microbes were taken in this procedure: two Gram-positive, *Staphylococcus aureus* and *Streptococcus mutans*, and one Gram-negative, *Pseudomonas aeruginosa*. These organisms were cultured on 20 ml Muller Hinton agar plates. Wells of approximately 10 mm was bored using a cutter. 250–1000 µg/ml of sample was taken. After 24 h of incubation at 37 °C, the plates were removed. The antibacterial activity was examined by measuring the diameter in millimeters of the inhibition zone formed around the well [45]. In this study, streptomycin was used as a standard antibacterial agent.

Cytotoxicity Assay: MTT Assay

In MTT assays, the reductase enzyme found in the mitochondria of living cells reduces the MTT reagent into purple formazan crystals, further soluble in DMSO. The absorbance of this colored solution is determined by measuring it at 570 nm with a reference wavelength of 630 nm. Because the reduction occurs only when mitochondrial reductase enzymes are active, the conversion rate can be directly related to the number of viable (living) cells. Cells treated with a drug can be tested for cytotoxicity by comparing their purple formazan production with untreated control cells. Hence, less purple would result if the drug affected cancer cells. In the same way, if the drug does not cause cytotoxicity, the mitochondrial reductase enzymes in live cells will convert MTT to purple formazan, producing a deeper purple color.

HeLa cells were used as a human cell line for the cytotoxicity test. HeLa cells were cultured with complete minimum essential medium (DMEM) (supplemented with 1% antibiotic solution (1X) and 10% FBS) in a T-25 flask for 2–3 passagesto maintain exponential growth. The cells were maintained in a CO_2 incubator with 5% CO_2, 37 °C, and a humidified atmosphere. The medium was carefully discarded upon reaching confluence, the flask was washed with 1X phosphate-buffered saline (1XPBS), and 1.5 ml trypsin was added. A complete DMEM solution of 1.5 ml was added to the flask to neutralize the trypsin after 2 min of incubation at 37 °C. The cells were centrifuged at 2000 rpm for 5 min and resuspended in 1 ml of complete DMEM. 10,000 cells per well were seeded in 96-well plates and incubated for 24 h in a CO_2 incubator.

The next day the depleted media was aspirated, and 2.5–12.5 µg/ml of D-CdS and uncapped CdS were added in triplicates for the treatment. Cells without drugs were kept as control, and without cells were put as blank. The plate was then incubated in a CO_2 incubator for 24 h. 10 µl of MTT reagent was added to each well and covered with aluminium foil (as MTT is light sensitive), followed by 3 h incubation at 37 °C. Removed the media carefully, and 100 µl of DMSO was added to each well. The plates were then placed on a platform shaker for 10–15 min to dissolve the formazan crystals. The absorbance was taken at 595 nm and 655 nm

as reference wavelengths using iMark Microplate Reader S/N 21988 [46]. The equation calculates the survivability percentage [19],

$$Survivability\ \% = \frac{sample\ average}{control\ average} \times 100$$

where sample average and control average mean that the blank corrected average value of difference of absorption value at 655 nm and 595 nm.

In Vitro Bioimaging of Cancer Cells

For bioimaging studies, HeLa cells, 1×10^4 cells per well, were cultured in a 96-well plate with coverslips and incubated overnight at 37 °C so that the cells were affixed to the surface of the cell-cultured plate. To this, 2.5 and 5 µg/mL D-CdS and uncapped CdS were added to the HeLa cells and incubated for 24 h. Cells without drugs were kept as control, and media without cells were kept blank. The plate was then incubated in a CO_2 incubator for 24 h. After 24 h of treatment, cells were viewed under a fluorescence microscope.

Results and Discussions

Characterizations of D-CdS

The formation of D-CdS was confirmed from their characterization data, including, UV–visible absorption, PL, XRD, and SEM.

UV–Visible Absorption Spectra

The UV–Visible absorption spectra of uncapped CdS and D-CdS are shown in Fig. 1. The absorption band of the CdS nanoparticles is observed in the wavelength range 425–515 nm with a well-defined maximum at 480 nm is attributed to the optical transition of the first excitonic state. The band gap energy (E_g) of CdS can be obtained using the formula: $E_g = 1240/\lambda$, where λ is the wavelength of the absorption edge. The calculated bandgap energy of CdS from the absorption edge is 2.58 eV. The maximum absorption peak of bulk CdS is at 499 nm with bandgap energy of 2.48 eV. Comparing this maximum excitonic wavelength with the absorption peak of bulk CdS, a blue shift in maximum absorption is observed due to the particle size reduction due to the quantum confinement of the photo-generated electron–hole pairs [47, 48]. It is also noted that CdS has non-zero absorption from 350 to 700 nm in the wavelength range. The particle size R can be obtained from Bru's formula [49],

$$E_g(R) = E_g(Bulk) + \frac{\hbar^2 \pi^2}{2R^2}\left[\frac{1}{m_e} + \frac{1}{m_h}\right] - \frac{1.786e^2}{\varepsilon R}$$
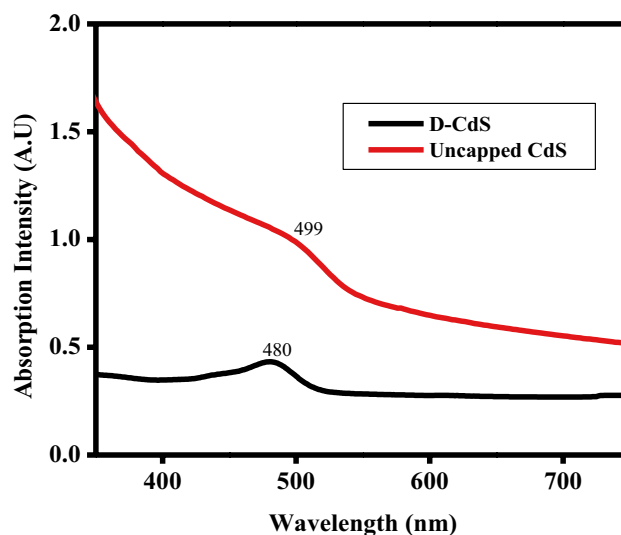

Fig. 1 UV–visible absorption spectra of uncapped and D-CdS

where $E_g(R)$ is the bandgap energy of the quantum dot, $E_g(Bulk)$ is the bandgap energy of bulk material R is the size of the quantum dot, and h is Plank's constant. m_e and m_h are the effective masses of the electron and hole respectively. e is the electron charge, ε is the relative dielectric constant of CdS ($\varepsilon = 8.9$). The calculated particle size is around 4 nm, which is a little smaller than that of the particle size observed by the SEM image; it may be due to the aggregation of particles while drying the samples.

XRD

The structural and morphological properties of CdS nanoparticles have been investigated by X-ray diffraction technique as shown in Fig. 2. XRD pattern gives information about the crystalline phase and crystalline size. The XRD pattern of CdS offers three prominent peaks at 2θ values of 26.70°, 44.20°, and 52.2°; the corresponding indexations could be at (111), (220), and, (311) which are evident in the cubic crystal structure (JCPDS file (10–454)). The broadened peaks show that the sizes of the particles are in the nano-range [50–54].

The crystallite size of CdS nanoparticles can be obtained from Scherrer's formula [55, 56]. The formula is given by

$$d = \frac{0.9\lambda}{\beta \cos\theta}$$

where d is the crystallite size in nm, λ is the wavelength of the X-rays used, 1.5406 Å, β is the full width at half maximum, and θ is the diffraction peak angle. The average crystalline size is obtained to be 1.5 nm, 2.3 nm, and 2.7 nm corresponding to the peaks of 26.70, 44.20, and 52.2 degrees respectively.

Fig. 2 XRD pattern of uncapped CdS and D-CdS
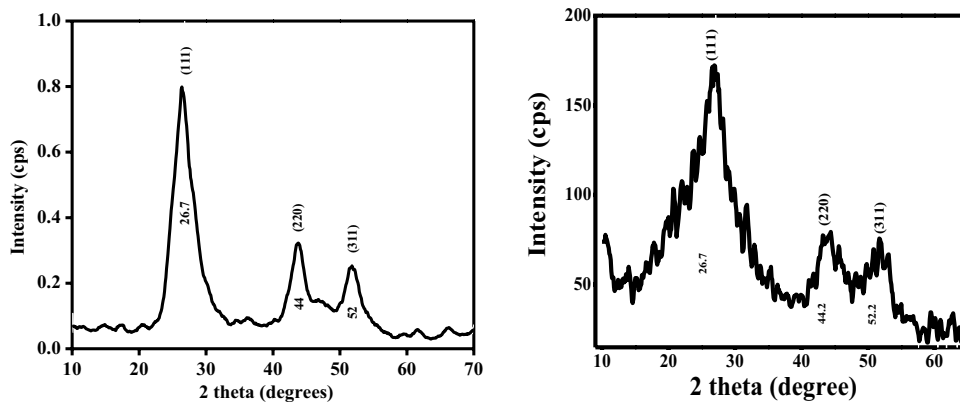
SEM

SEM image is recorded for D-CdS and is presented in Fig. 3. The micrograph of D-CdS shows spherical morphology. The average diameter of the D-CdS is found to be 10 nm and that of uncapped CdS is above 50 nm.

Photoluminescence of D-CdS

The photoluminescence (PL) spectra of uncapped CdS and D-CdS are demonstrated in Fig. 4. Emission spectra of D-CdS show two peaks in the range of 450 nm to 600 nm for an excitation wavelength of 400 nm. The first higher peak was centered at 486 nm and the second lower peak was centered at 541 nm. The peak at 486 nm is attributed to the emission from the absorption edge. The corresponding bandgap energy 2.5 eV, which is an increased value compared to the bandgap energy of bulk CdS (2.42 eV). This is due to the particle size reduction as a result of quantum confinement of the photo-generated electron–hole pairs [45]. The peak at 541 nm may be corresponds to emission due to surface states or traps associated crystalline defects. Here, in the CdS nanoparticles, this emission is linked to cadmium and sulfur atom vacancies [57–59]. The uncapped CdS has also two peaks, one is at 491 nm and the second one is at 549 nm. The peaks of D-CdS are blue-shifted as compared to uncapped CdS. This blue shifting is due to the quantum confinement effect of D-CdS. A considerable amount of enhancement in the fluorescence intensity of D-CdS was noted. This may be due to the presence of Schiff base ligand which is highly fluorescent around the wavelength of 500 nm, which matches the emission wavelength of CdS nanoparticles.

As the synthesized D-CdS possess emission wavelength in visible region and considering the biocompatibility,
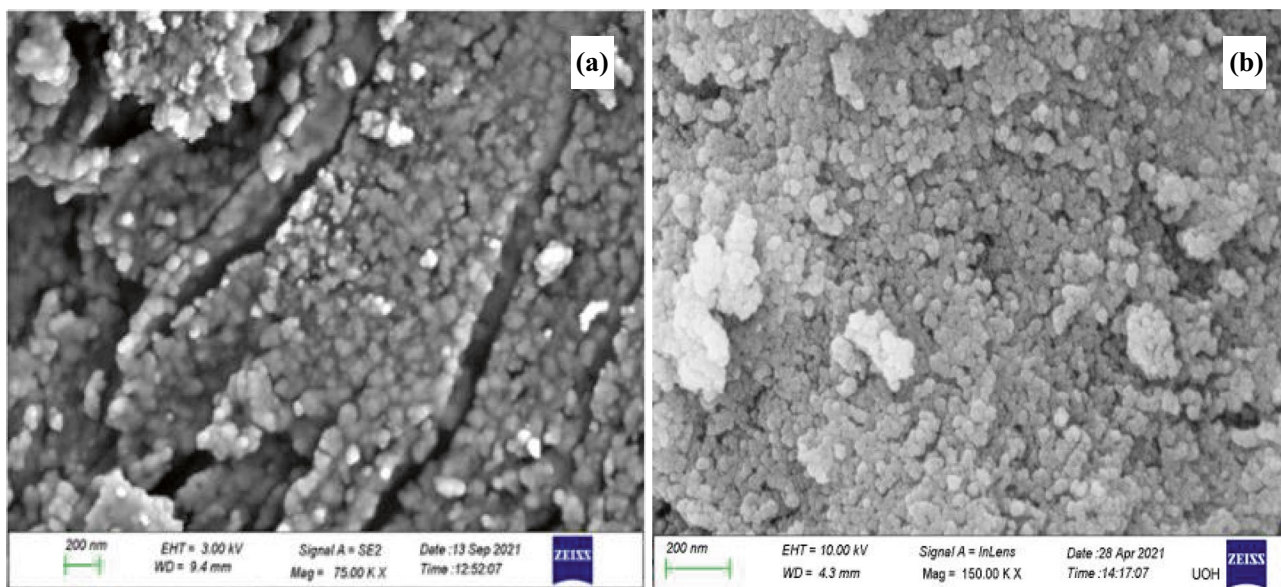

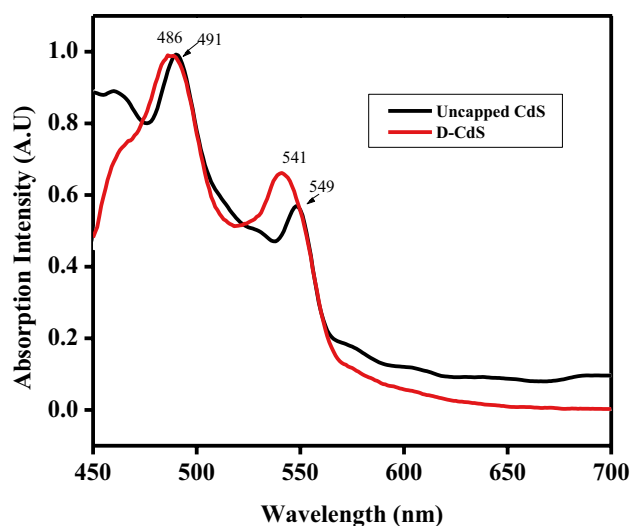**Fig. 3** SEM images of **a** Uncapped CdS and **b** D-CdS

Fig. 4 PL spectra of Uncapped CdS and D-CdS

fluorescence cell imaging may be a key application. Also, due to the multiple emission wavelengths, D-CdS can be employed for the production of multicoloured light emitting diodes [47].

Photocatalytic Studies of D-CdS

The photocatalytic degradation of Rhodamine 6G and Methylene blue was studied in the presence and absence of D-CdS under UV irradiation, for a period of 120 min. The absorption peak of Rhodamine 6G at 520 nm and absorption peak of Methylene blue at 665 nm were considered to demonstrate the photocatalytic activity. Figure 5a shows the absorption spectra of Rhodamine 6G in the absence of D-CdS. The peak corresponding to 520 nm is due to the transition between S0 to S1 [50]. Figure 5b shows the absorption spectra of Rhodamine 6G in the presence of photocatalyst. It was observed that decrement in the intensity of maximum absorption was very less in the absence of D-CdS after 120 min UV irradiation. It is observed that the percentage of degradation (Fig. 5c) of Rhodamine 6G increased in the presence of the photocatalyst; 64% degradation occurred within 120 min. At the same time, only 7% of degradation happened without a photocatalyst.

Figure 6a, b demonstrate the absorption spectra of Methylene blue in the absence and presence of D-CdS respectively. The maximum absorbance takes place in the range of 550 nm to 700 nm with a pair of characteristic peaks at 612 nm and 665 nm. The peak at 665 nm is due to π-π* transition associated with the resonance of the π electrons from sulphur resonating with those from carbons in thiazinic center. The peak at 612 nm corresponds to π-π* transition of benzene
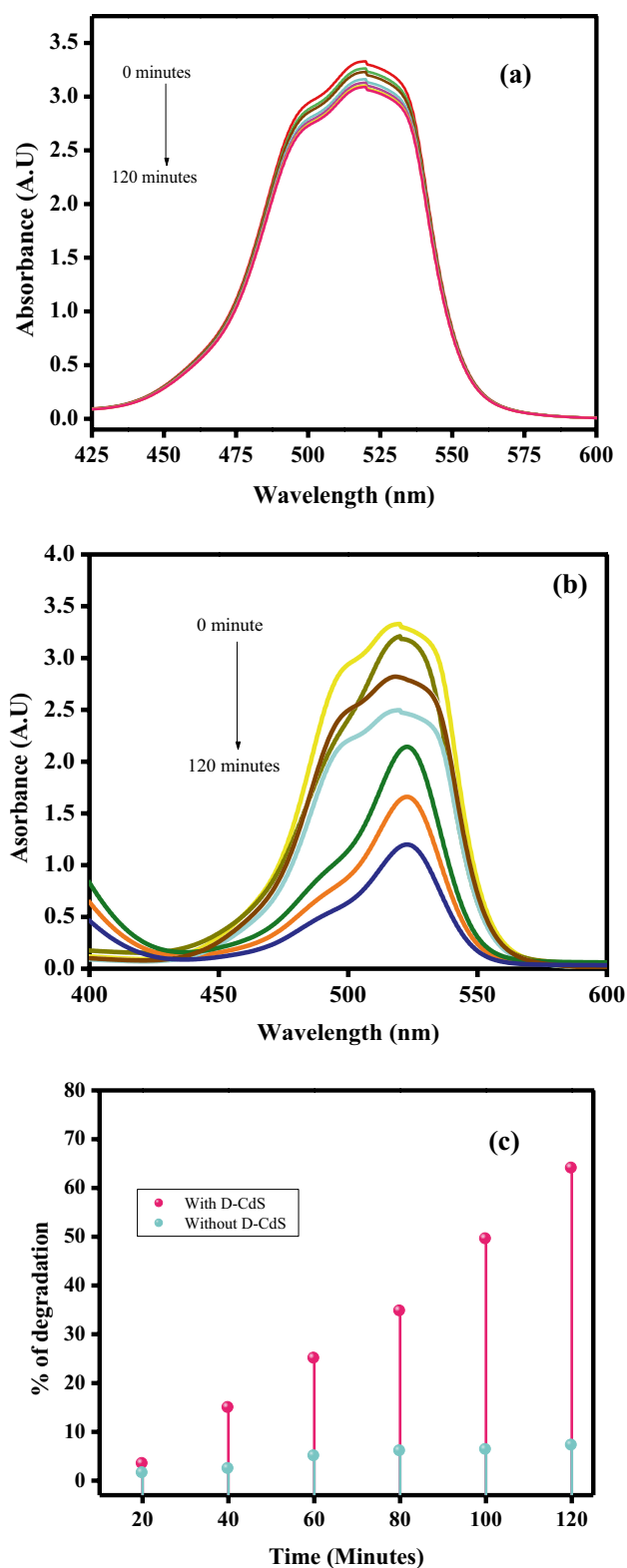

Fig. 5 Photocatalytic degradation of Rhodamine 6G in the **a** absence and **b** presence of photocatalyst under UV irradiation **c** percentage of degradation with and without photocatalyst
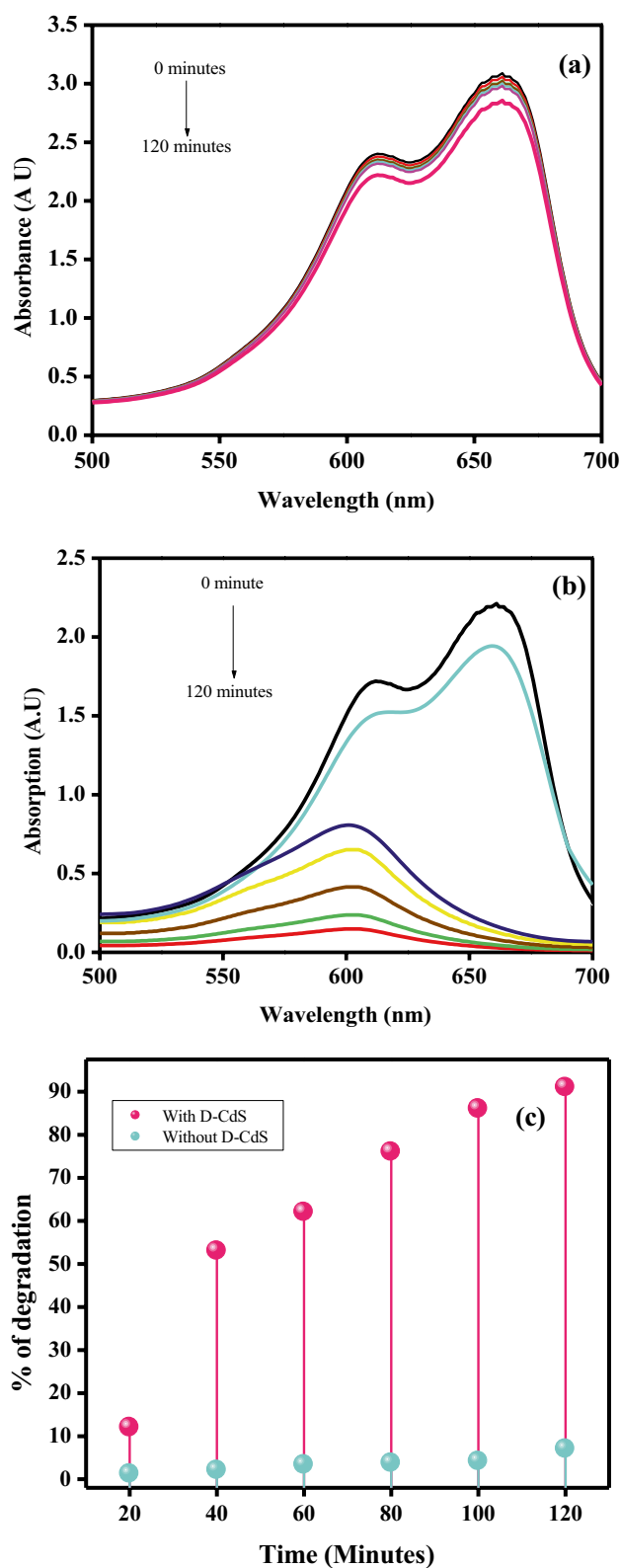
Fig. 6 Photocatalytic degradation of Methylene blue in the **a** absence and **b** presence of catalyst under UV irradiation **c** percentage of degradation with and without photocatalyst

rings [60]. According to Fig. 6c, in the absence of catalyst, 12% degradation occurred for both peaks within 120 min. In the presence of a photocatalyst, within 120 min, 91% of degradation occurred for the peak at 612 nm whereas, 98.9% degradation occurred for the peak at 665 nm.

D-CdS is found to be a potential photocatalyst for Methylene blue. The photodegradation of Methylene blue is greater than that of Rhodamine 6G, possibly due to Rhodamine 6G's higher photostability. Photocatalytic mechanism of D-CdS is instigated by irradiation by UV light. Excitation of electrons from the valence band to the conduction band of CdS, results in the production of electron–hole pairs [61]. In addition to longer charge carrier lifetimes, CdS nanoparticles show better redox properties because the photo-generated electrons and holes are inhibited under UV irradiation. OH radicals are formed when the holes in CdS react with water molecules or hydroxide ions. The OH radicals are effective oxidizing agent, and it attacks organic pollutants present at the surface of CdS. The possible mechanism of photocatalytic reactions of R6G and Methylene blue as follows:

$$CdS + h\upsilon \rightarrow CdS + h^+ + e^-$$

$$h^+ + H_2O \rightarrow OH^- + H^+$$

$$h^+ + OH^- \rightarrow OH^{\cdot}$$

$$O_2 + e^- \rightarrow O_2^-$$

$$2H_2O + O_2^- + e^- \rightarrow 2OH + 2OH^-$$
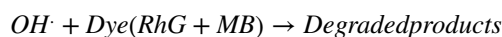
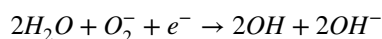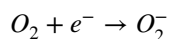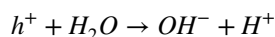$$OH^{\cdot} + Dye(RhG + MB) \rightarrow Degraded products$$

Table 1 represents the percentage of degradation of various dyes in the presence of differently prepared CdS nanoparticles. Comparison may not be effective because the dissimilarity in dyes, irradiation time and irradiation source.

Antibacterial Activities

The experimental details for the antimicrobial studies were presented in the experimental section. The antimicrobial activities of the prepared samples, D-CdS and uncapped CdS were investigated by disc diffusion method using Pseudomonas aeruginosa, Staphylococcus aureus, (Gram-positive) and Streptococcus mutans (Gram-negative). The D-CdS and uncapped CdS are exhibiting inhibition to both Gram—positive and Gram-negative pathogenic bacteria. The diameter of inhibition zone was measured for 1 mg/ml concentration. Table 2 shows the inhibition zone diameter

Table 1 Data of photocatalytic activity of various CdS nanoparticles

Photocatalyst	Synthesis method (Morphology)	Dye	Wavelength of irradiation (nm)	% of degradation (Irradiation time)	Reference
CdS	Biogenic synthesis (Spherical)	Methylene blue	365	37.15% (60 min)	[62]
CdS@CP	Recycled Cadmium from waste water (Mixed phase of hexagonal and cubic)	Rhodamine B	Visible light	99% (90 min)	[63]
L-CdS	Schiff base capped CdS (spherical)	Rhodamine 6G and Methylene blue	245	70% and 98% (120 min)	[42]
CdS	Template free synthesis (nano spheres and nano hollow spheres	Methylene blue	visible	100% (300–400 min)	[64]
CdS	Hydrothermal route (spherical)	Eosin red, Congo red, and Methylene blue	visible	91% (100 min) 85% (120 min) 73% (180 min)	[65]
CdS	Wet chemical method under reflux condition assisted by thioglycollic acid (nanorod)	Methyl orange	Mercury lamp	93% (40 min)	[66]
CdS	Schiff base capped (different shaped)	Methyl red	Visible	100% (4 h)	[61]
D-CdS	DNA capped (spherical)	Rhodamine 6G and Methylene blue	245	64% and 91% (120 min)	-

for the samples at 1 mg/ml concentration. D-CdS shows better activity towards Gram-negative bacteria, Pseudomonas aeruginosa. Gram—positive bacteria consists of a thick peptidoglycan cell wall (monoderms). Gram negative bacteria have much thinner peptidoglycan cell wall and in addition they have an outer membrane containing lipopolysaccharides surrounding the cell wall (diderms). Lipopolysaccharides consist of lipids and polysaccharides. Polysaccharides are polymeric carbohydrates composed of long chains of monosaccharide units joined by glycosidic linkages. Lucas et al. explained the interaction between carbohydrates and DNA [67]. Here in our work, the antibacterial sample consists of DNA capped CdS nanoparticles. Once the D-CdS introduced into the bacteria, it can interact with the outer layer, lipopolysaccharides, of Gram-negative bacteria much faster than in Gram-positive bacteria. The particle size reduction and DNA biotemplate effect make the D-CdS more active than uncapped CdS. Figure 7 represents the antibacterial activity images of CdS in different concentrations.

Table 2 Antibacterial activity of uncapped CdS and D-CdS

Species	Zone diameter (mm) Concentration (1 mg/ml)		
	D-CdS	Uncapped CdS	Standard (Streptomycin) (100 μg/ml)
Pseudomonas aeruginosa	24	12	29
Staphylococcus aureus	20	12	27
Streptococcus mutans	17	11	25

Cytotoxicity analysis: MTT Assay

Cytotoxic effect of D-CdS, and uncapped CdS against HeLa cell lines was examined within 24 h. Figure 8 shows the MTT assay results with concentration versus cell survival rate. D-CdS shows considerable toxicity towards HeLa cells.

In Fig. 9a, b, the cell viabilities of the uncapped CdS and D-CdS respectively for different concentrations are shown. Figure 9 implies that inhibition of HeLa cells are steadily enhanced with uncapped CdS and D-CdS concentration i.e., both of them exhibit a dose-dependent toxicity. The LC_{50} value of uncapped CdS is found to be 2.4 μg/ml. At a concentration 2.5 μg/ml, it shows 84% cell viability and 43% viability 12.5 μg/ml. The calculated LC_{50} value is equal to 8 μg/ml.

The LC_{50} value of uncapped CdS on HeLa cells reported by Susha Naranthatta et al., is 7 μg/ml. In another report, SkTofajjen Hossain et al., LC_{50} value of uncapped CdS is observed to be 4 μg/ml. Reyes-Esparza et al. reported an improved biocompatibility in dextrin-capped CdS nanoparticles than uncapped CdS. According to them, a concentration less than 1 μg/mL is not at all toxic to HeLa cells. The concentrations taken in this work is much higher than this. Therefore, DNA, the capping agent to CdS can improve biocompatibility by reducing the toxicity of unmodified CdS. Here the LC_{50} value of D-CdS is much greater than that of uncapped CdS, which indicates that toxicity reduced considerably for D-CdS. Toxicity and LC_{50} value are inversely proportional.

As CdS nanoparticles possess photoluminescence in the visible range of wavelength, the biocompatible D-CdS can effectively be used as potential candidate for in vitro cellular imaging (bioimaging).
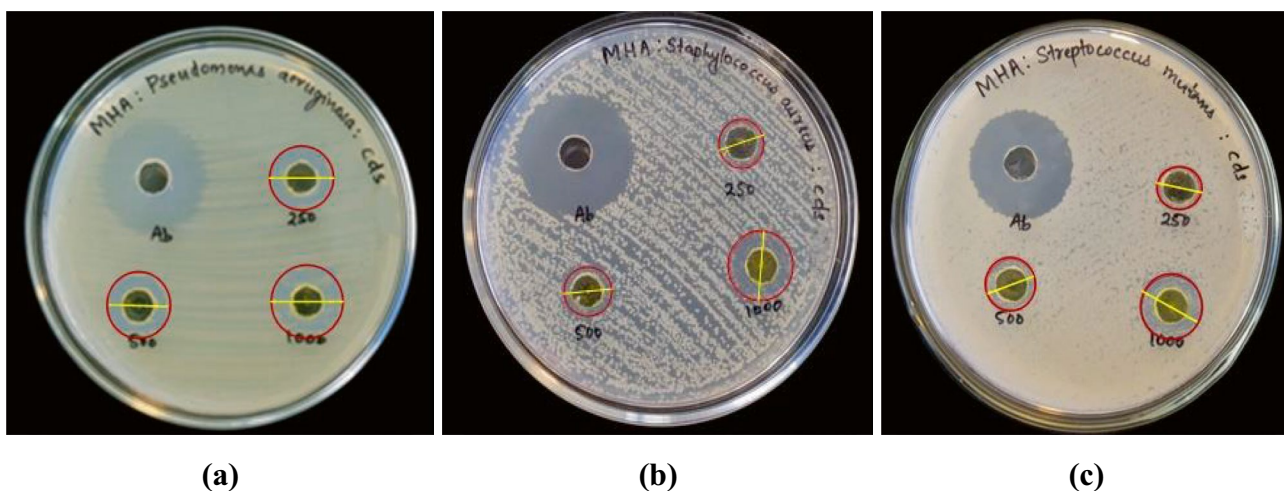
Fig. 7 Antibacterial test results of *Pseudomonas aeruginosa, Staphylococcus aureus and Streptococcus mutans* after 24 h incubation by D-CdS (**a**–**c**). Streptomycin used as control
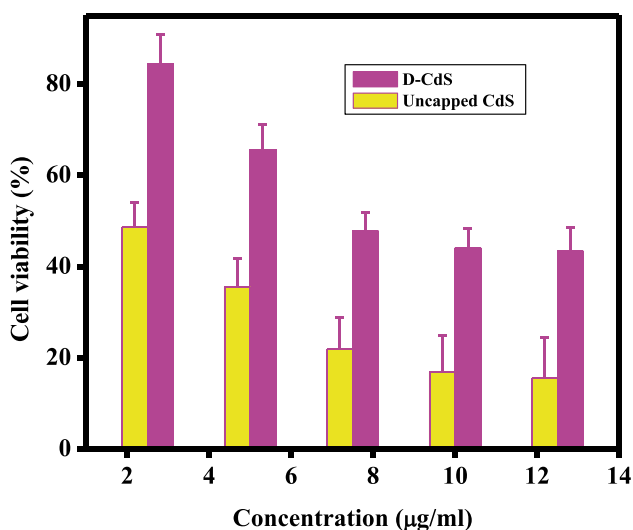

Fig. 8 Histogram of cell viability in the presence of uncapped CdS and D-CdS

Bioimaging

Cellular imaging of D-CdS is one of the vital features of this study. For this, HeLa cells were treated with 2.5 µg/ml D-CdS and uncapped CdS, which is a less value than LC_{50} of D-CdS. After 24 h of treatment, cells were viewed under a fluorescence microscope. The cell membrane, a double-layered lipid, detaches the cytoplasm from the surroundings. Figure 10a, b shows the bright field images of the HeLa cells treated with 2.5 µg/ml of uncapped CdS and D-CdS respectively. For a concentration study of D-CdS, 5 µg/ml was also taken in to consideration. Figure 10c shows the bright field image of HeLa cells treated with 5 µg/ml D-CdS.

The cells are clearly seen from the bright-field images. Cells with round shape represent cell death. It is obvious from the Fig. 10a that more cells were destroyed in the presence of uncapped CdS which due to its high toxicity. Image is very unclear due to the presence of bigger sized CdS

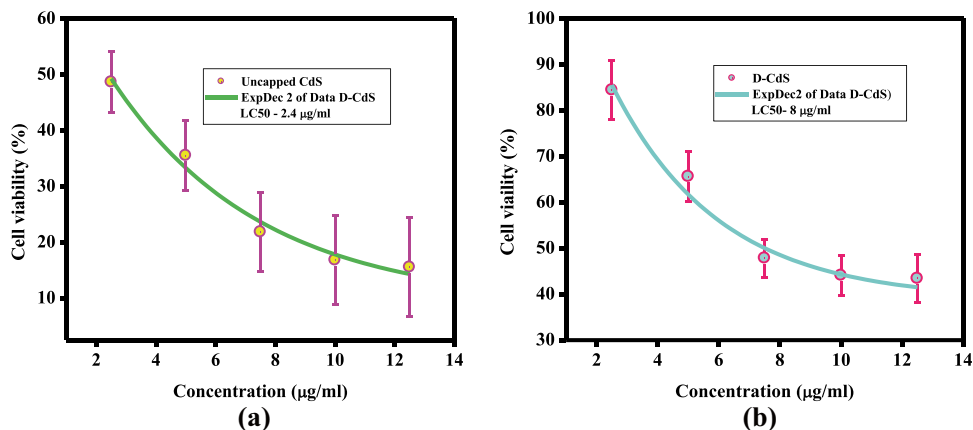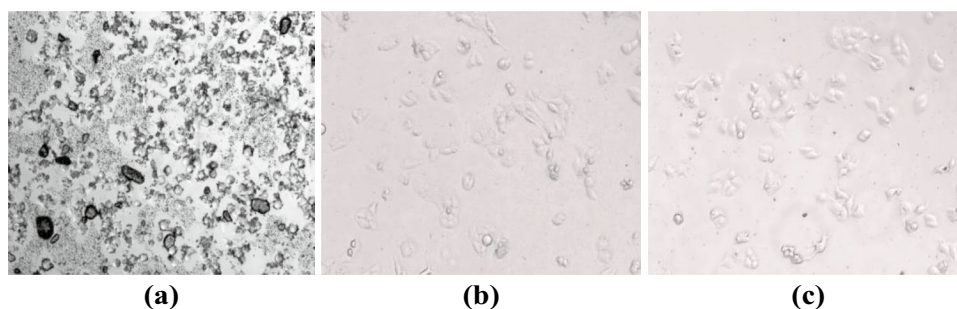**Fig. 9** Cell viability **a** exponential fit uncapped CdS **b** D-CdS

Fig. 10 Bright-field images of HeLa cells in the presence of **a** Uncapped CdS 2.5 µg/ml **b** D-CdS 2.5 and **c** D-CdS 5 µg/ml. Cell death is visible by the round shape of the cell

(a) **(b)** **(c)**

nanoparticles. This uncapped CdS were not much soluble in any solvents. Therefore, it is not a desirable candidate for bioimaging. In Fig. 10b, cells are destroyed in the presence of D-CdS (2.5 µg/ml) Even though the cell death rate is lesser than that of uncapped CdS, cells are very clearly seen and not blurred in the presence of D-CdS. D-CdS were easily soluble in DMSO. It proves that D-CdS is a promising candidate for bioimaging. It is obvious from the Fig. 10b, c that D-CdS shows a dose-dependent toxicity as seen from MTT assay. Higher number of cell death happened for a higher concentration.

Conclusion

In this work we report photocatalytic, antibacterial, cytotoxic, and bioimaging applications of D-CdS nanoparticles. It was found that D-CdS is a potential photodegrading agent for Rhodamine 6G and Methylene blue dye with photodegradation of 64% and 91% respectively. Antibacterial activity of D-CdS nanoparticles was found to be better enough than uncapped CdS nanoparticles ad found that both of them show higher activity towards G-negative bacteria, *Pseudomonas aeruginosa*. The cytotoxicity of the CdS nanoparticles were assessed via the MTT assay, proved that the D-CdS is less toxic than uncapped CdS. D-CdS shows 84% cell viability in 2.5 µg/ml whereas uncapped CdS shows only 48% cell viability. In vitro cellular imaging applications of prepared D-CdS are also investigated and found that D-CdS shows dose dependent toxicity. The results confirm that D-CdS is a potential photocatalyst, antibacterial agent and excellent biocompatible nanoparticles for bioimaging applications.

Authors' Contributions All authors contributed to the study conception and design. Material preparation, data collection and analysis were performed by Reena V N, Shilpa T, Aswati Nair R, Bhagyasree G S, Misha H and Nithyaja B. The first draft of the manuscript was written by Reena V N and all authors commented on previous versions of the manuscript. All authors read and approved the final manuscript.

Availability of Data and Materials The data that support the findings of this study are available from the corresponding author upon reasonable request.

Declarations

Ethical Approval Not Applicable.

Competing Interests No financial interests to declare.

References

1. Braun E, Eichen Y, Sivan U, Ben-Yoseph G (1998) DNA-templated assembly and electrode attachment of a conducting silver wire. Nature 391:775
2. Liu Z, Yuangang Zu, Yujie Fu, Zhang Y, Liang H (2008) Growth of the oxidized nickel nanoparticles on a DNA template in aqueous solution. Mater Lett 62:2315
3. Yao Y, Song Y, Wang Li (2008) Synthesis of CdS nanoparticles based on DNA network templates. Nanotechnology 19:405601
4. Wei G, Wang Li, Liu Z, Song Y, Sun L, Tao Y, Liz Z (2005) DNA-network-templated self assembly of silver nanoparticles and their application in surface enhanced Raman scattering. J Phys Chem B 109:23941
5. Zhu XL, Junji H-Y (2001) Electrochemical preparation of silver dendrited in the presence of DNA. Mater Res Bull 36:1687
6. Radhika NK, Kavitha BS, Asokan S, Gorthi SS (2020) Detection of copper nanoparticles templated by DNA using etched fibre bragg grating sensor. IEEE Sens J 20(16):9179–9186
7. Tan SJ, Kahn JS, Derrien TL, Campolongo MJ, Zhao M, Smilgies DM, Luo D (2014) Crystallization of DNA-capped gold nanoparticles in high-concentration, divalent salt. Environ Angew Chem 126(5):1340–1343
8. Jyothi PP, Anitha B, Smitha S, Vibitha BV, Krishna PA, Tharayil NJ (2020) DNA-assisted synthesis of nanoceria, its size dependent structural and optical properties for optoelectronic applications. Bull Mater Sci 43:1–7
9. Banerjee R, Jayakrishnan R, Ayyub P (2000) Effect of the size-induced structural transformation on the band gap in CdS nanoparticles. J Phys Condens Matter 12:10647. https://doi.org/10.1088/0953-8984/12/50/325
10. Murugan AV, Sonawane RS, Kale BB, Apte SK, Kulkarni AV (2001) Microwave–solvothermal synthesis of nanocrystalline cadmium sulfide. Mater Chem Phys 71:98–102. https://doi.org/10.1016/S0254-0584(00)00533-2
11. El-Din MG (2020) Pristine and engineered biochar for the removal of contaminants coexisting in several types of industrial

wastewaters: a critical review. Sci Total Environ 809:151120. https://doi.org/10.1016/j.scitotenv.2021.151120

12. Zampeta C, Bertaki K, Triantaphyllidou IE, Frontistis Z, Vayenas DV (2021) Treatment of real industrial-grade dye solutions and printing ink wastewater using a novel pilot-scale hydrodynamic cavitation reactor. J Environ Manag 297:1. https://doi.org/10.1016/j.jenvman.2021.113301

13. Long W, Hamza MU, Abdul-Fattah MN, Rheima AM, Ahmed YM, Fahim FS, Fakhri A (2022) Preparation, photocatalytic and antibacterial studies on novel doped ferrite nanoparticles: Characterization and mechanism evaluation. Colloids Surf A Physicochem Eng Asp 650:129468. https://doi.org/10.1016/j.colsurfa.2022.129468

14. Paziresh F, Salem A, Salem S (2021) Super effective recovery of industrial wastewater contaminated by multi-disperse dyes through hydroxyapatite produced from eggshell. Sustain Chem Pharm 23:100501. https://doi.org/10.1016/j.scp.2021.100501

15. Bahadoran A, Baghbadorani NB, De Lile JR, Masudy-Panah S, Sadeghi B, Li J, Fakhri A (2022) Ag doped Sn_3O_4 nanostructure and immobilized on hyperbranched polypyrrole for visible light sensitized photocatalytic, antibacterial agent and microbial detection process. J Photochem Photobiol B Biol 228:112393

16. Youssef Z, LudovicColombeau SA (2018) Dye-sensitized nanoparticles for heterogeneous photocatalysis: cases studies with TiO2, ZnO, fullerene and graphene for water purification. Dyes Pigments 159:49–71. https://doi.org/10.1016/j.dyepig.2018.06.002

17. Wei G, Basheer C, Jiang Z (2016) Visible light photocatalysis in chemoselective functionalization of C (sp^3)H bonds enabled by organic dyes. Tetrahedron Lett 57:3801–3809. https://doi.org/10.1016/j.tetlet.2016.07.032

18. Jabbar ZH, Ebrahim SE (2022) Recent advances in nano-semiconductors photocatalysis for degrading organic contaminants and microbial disinfection in wastewater: A comprehensive review. Environ Nanotechnol Monit Manag 17:100666

19. Naranthatta S, Janardhanan P, Pilankatta R, Nair SS (2021) Green synthesis of engineered CdS nanoparticles with reduced cytotoxicity for enhanced bioimaging application. ACS Omega 6:8646–8655

20. Shivaji K, Mani S, Ponmurugan P, De Castro CS, Lloyd Davies M, Balasubramanian MG, Pitchaimuthu S (2018) Green-synthesis-derived CdS quantum dots using tea leaf extract: antimicrobial, bioimaging, and therapeutic applications in lung cancer cells. ACS Appl Nano Mater 1:1683–1693

21. Hong L, Cheung TL, Rao N, Ouyang Q, Wang Y, Zeng S, Yang C et al (2017) Millifluidic synthesis of cadmium sulfide nanoparticles and their application in bioimaging. RSC Adv 7:36819–36832

22. Kulkarni SK, Ethiraj AS, Kharrazi S, Deobagkar DN, Deobagkar DD (2005) Synthesis and spectral properties of DNA capped CdS nanoparticles in aqueous and non-aqueous media. Biosens Bioelectron 21(1):95–102

23. Ma N, Yang J, Stewart KM, Kelley SO (2007) DNA-passivated CdS nanocrystals: luminescence, bioimaging, and toxicity profiles. Langmuir 23(26):12783–12787. https://doi.org/10.1021/la7017727

24. Yao Y, Song Y, Wang L (2008) Synthesis of CdS nanoparticles based on DNA network templates. Nanotechnology 19:405601. https://doi.org/10.1088/0957-4484/19/40/405601

25. Nithyaja B, Vishnu K, Mathew S, Radhakrishnan P, Nampoori VP (2012) Studies on CdS nanoparticles prepared in DNA and bovine serum albumin based biotemplates. J Appl Phys 112:064704. https://doi.org/10.1063/1.4752750

26. Reena VN, Misha H, Bhagyasree GS, Nithyaja B (2022) Enhanced photoluminescence and color tuning from Rhodamine 6G-doped sol–gel glass matrix via DNA templated CdS nanoparticles. AIP Adv 12(10):105217. https://doi.org/10.1063/5.0123529

27. Kanude KR, Jain P (2017) Biosynthesis of CdS nanoparticles using Murraya Koenigii leaf extract and their biological studies. Int J Sci Res Multidiscip Stud 3:5–10

28. Borovaya MN, Naumenko AP, Matvieieva NA, Blume YB, Yemets AI (2014) Biosynthesis of luminescent CdS quantum dots using plant hairy root culture. Nanoscale Res Lett 9:1–7

29. Kakanejadifard A, Khojasteh V, Zabardasti A, Azarbani F (2018) New azo-schiff base ligand capped silver and cadmium sulfide nanoparticles preparation, characterization, antibacterial and antifungal activities. Organic Chemistry Research 4:210–226

30. Ahamad T, Khan M, Kumar S, Ahamed M, Shahabuddin M, Alhazaa AN (2016) CdS quantum dots: growth, microstructural, optical and electrical characteristics. Appl Phys B 122:1–8. https://doi.org/10.1007/s00340-016-6455-3

31. Maity R, Chattopadhyay KK (2006) Synthesis and optical characterization of CdS nanowires by chemical process. J Nanopart Res 8:125. https://doi.org/10.1007/s11051-005-8595-y

32. Zhang YC, Wang GY, Hu XY (2007) Solvothermal synthesis of hexagonal CdS nanostructures from a single-source molecular precursor. J Alloys Compd 437:47

33. Ma X, Xu F, Liu Y, Liu X, Zhang Z, Qian Y (2005) Double-dentate solvent-directed growth of multi-armed CdS nanorod-based semiconductors. Mater Res Bull 40:2180–2188. https://doi.org/10.1016/j.materresbull.2005.07.009

34. Wang Y, To CY, Ng DHL (2006) Controlled synthesis of CdS nanobelts and the study of their cathodoluminescence. Mater Lett 60:1151–1155. https://doi.org/10.1016/j.matlet.2005.10.098

35. Wang S, Jarrett BR, Kauzlarich SM, Louie AY (2007) Core/shell quantum dots with high relaxivity and photoluminescence for multimodality imaging. J Am Chem Soc 129:3848–3856. https://doi.org/10.1021/ja065996d

36. Böer KW (2010) CdS enhances Voc and fill factor in CdS/CdTe and $CdS/CuInSe_2$ solar cells. J Appl Phys 107:023701. https://doi.org/10.1063/1.3256190

37. Stouwdam JW, Janssen RA (2009) Electroluminescent Cu-doped CdS quantum dots. Adv Mater 21(28):2916–2920. https://doi.org/10.1002/adma.200803223

38. Liu ZF, Li YJ, Zhao Z, Cui Y, Hara K, Miyauchi M (2010) Block copolymer templated nanoporous TiO 2 for quantum-dot-sensitized solar cells. J Mater Chem 20(3):492–497. https://doi.org/10.1039/B917634A

39. Ma RM, Wei XL, Dai L, Huo HB, Qin GG (2007) Synthesis of CdS nanowire networks and their optical and electrical properties. Nanotechnology 18:205605. https://doi.org/10.1088/0957-4484/18/20/205605

40. Pradhan N, Battaglia DM, Liu Y, Peng X (2008) Efficient, stable, small, and water-soluble doped ZnSe nanocrystal emitters as non-cadmium biomedical labels. Nano Lett 14:312–317. https://doi.org/10.1021/nl062336y

41. Ghosh B, Das M, Banerjee P, Das S (2008) Fabrication of vacuum-evaporated SnS/CdS heterojunction for PV applications. Sol Energy Mater Sol Cells 92:1099–1104. https://doi.org/10.1016/j.solmat.2008.03.016

42. Reena VN, Kumar KS, Shilpa T, Aswati Nair R, Bhagyasree GS, Nithyaja B (2023) Photocatalytic and enhanced biological activities of schiff base capped fluorescent CdS nanoparticles. J Fluoresc 1–14. https://doi.org/10.1007/s10895-023-03193-4

43. Xu B, Ahmed MB, Zhou JL, Altaee A (2020) Visible and UV photocatalysis of aqueous perfluorooctanoic acid by TiO2 and peroxymonosulfate: Process kinetics and mechanistic insights. Chemosphere 243:125366

44. Ayodhya D, Veerabhadram G (2019) Fabrication of Schiff base coordinated ZnS nanoparticles for enhanced photocatalytic degradation of chlorpyrifos pesticide and detection of heavy metal ions. J Materiomics 5:446–454

45. Reena VN, Kumar KS, Bhagyasree GS, Nithyaja B (2022) One-pot synthesis, characterization, optical studies and biological activities of a novel ultrasonically synthesized Schiff base ligand and its Ni (II) complex. Results Chem 4:100576

46. National Committee for Clinical Laboratory Standards Fifth Edition Approved Standard M2–A5 NCCLS, Villanova, PA (1993)

47. Sakr MA, Gawad SAA, El-Daly SA, Abou Kana MT, Ebeid EZM (2019) Laser behavior of (E, E)-2, 5-Bis 2-(1-methyl-1H-Pyrrole-2-Yl pyrazine (BMPP) dye hybridized with CdS quantum dots (QDs) in sol-gel matrix and various hosts. Res J Nanosci Eng 3(2):1–12

48. Shoujun LAI, Xijun CHANG, Sui WANG, Jie MAO, Lei TIAN (2009) Studies on the interaction between CdS quantum dots and organic dyes: Absorbtion and fluorescence spectroscopy. Rev Roum Chim 54(10):815–822

49. Brus LE (1984) Electron–electron and electron-hole interactions in small semiconductor crystallites: The size dependence of the lowest excited electronic state. J Chem Phys 80:4403–4409. https://doi.org/10.1063/1.447218

50. Dorset DL (1998) X-ray diffraction: a practical approach. Microsc Microanal 4(5):513–515. https://doi.org/10.1017/S143192769800049X

51. Maddalena R, Hall C, Hamilton A (2018) Effect of silica particle size on the formation of calcium silicate hydrate using thermal analysis. Thermochim Acta. https://doi.org/10.1016/j.tca.2018.09.003

52. Wang W, Germanenko I, Samy El-Shall M (2002) Room-temperature synthesis and characterization of nanocrystalline CdS, ZnS, and $Cd_xZn_{1-x}S$. Chem Mater 14:3028. https://doi.org/10.1021/cm020040x

53. Devi R, Purkayastha P, Kalita PK, Sarma B (2007) Synthesis of nanocrystalline CdS thin films in PVA matrix. Bull Mater Sci 30:123–128. https://doi.org/10.1007/s12034-007-0022-9

54. Sabah A, Siddiqi SA, Ali S (2010) Fabrication and characterization of CdS nanoparticles annealed by using different radiations. World Acad Sci 4(9):532–539. https://doi.org/10.5281/zenodo.1330301

55. Rathore KS, Deepika DP, Saxena NS, Sharma KB (2009) Effect of Cu doping on the structural, optical and electrical properties of CdS nanoparticles. J Ovonic Res 5(6):175–185

56. Meron T, Markovich G (2005) Ferromagnetism in colloidal Mn^{2+}-doped ZnO nanocrystals. J Phys Chem B 109:20232. https://doi.org/10.1021/jp0539775

57. López-Cabaña Z, Sotomayor Torres CM, González G (2011) Semiconducting properties of layered cadmium sulphide-based hybrid nanocomposites. Nanoscale Res Lett 6:1–8. https://doi.org/10.1186/1556-276X-6-523

58. Cao H, Wang G, Zhang S, Zhang X, Rabinovich D (2006) Growth and optical properties of wurtzite-type CdS nanocrystals. Inorg Chem 45:5103–5108. https://doi.org/10.1021/ic060440c

59. Wu JC, Zheng J, Wu P, Xu R (2011) Study of native defects and transition-metal (Mn, Fe Co, and Ni) doping in a zinc-blende CdS photocatalyst by DFT and hybrid DFT calculations. J Phys Chem C 115:5675–5682

60. Khan A, Khan R, Waseem A, Iqbal A, Shah ZH (2016) CdS nano-capsulesand nanospheres as efficient solar light-driven photocatalysts for degradation of Congo red dye. Inorg Chem Commun 72:33–41. https://doi.org/10.1016/j.inoche.2016.08.001

61. Ayodhya D, Veerabhadram G (2017) One-pot green synthesis, characterization, photocatalytic, sensing and antimicrobial studies of Calotropis gigantea leaf extract capped CdS NPs. Mater Sci Eng B Solid-State Mater Adv Technol 225:33–44. https://doi.org/10.1016/j.mseb.2017.08.008

62. Bhadwal RK, Tripathi AS, Gupta RM (2014) Biogenic synthesis and photocatalytic activity of CdS nanoparticle. RSC Adv 4:9484–9490. https://doi.org/10.1039/C3RA46221H

63. Li JX, Zhang RL, Pan ZJ, Liao Y, Xiong CB, Chen ML, Huang R, Pan XH, Chen Z (2021) Preparation of CdS@ C photocatalyst using phytoaccumulation Cd recycled from contaminated wastewater. Front Chem 9:717210. https://doi.org/10.3389/fchem.2021.717210

64. Lin G, Zheng J, Rong Xu (2008) Template-free synthesis of uniform CdS hollow nanospheres and their photocatalytic activities. J Phys Chem C 112(19):7363–7370. https://doi.org/10.1021/jp8006969

65. Yu Z, Yin B, Fengyu Qu, Xiang Wu (2014) Synthesis of self-assembled CdS nanospheres and their photocatalytic activities by photodegradation of organic dye molecules. Chem Eng J 258:203–209. https://doi.org/10.1016/j.cej.2014.07.041

66. Chen F, Jia D, Cao Y, Jin X, Liu A (2015) Facile synthesis of CdS nanorods with enhanced photocatalytic activity. Ceram Int 41(10):14604–14609. https://doi.org/10.1016/j.ceramint.2015.07.179

67. Lucas R, Gomez-Pinto I, Avino A, Reina JJ, Eritja R, Gonzalez C, Morales JC (2011) Highly polar carbohydrates stack onto DNA duplexes via CH/π interactions. J Am Chem Soc 133(6):1909–1916. https://doi.org/10.1021/ja108962j